ADVANCED FUNCTIONAL MATERIALS
www.afm-journal.de

Check for updates

A Modeling Framework for Jamming Structures

*Buse Aktaş, Yashraj S. Narang, Nikolaos Vasios, Katia Bertoldi, and Robert D. Howe**

Jamming is a structural phenomenon that provides tunable mechanical behavior. A jamming structure typically consists of a collection of elements with low effective stiffness and damping. When a pressure gradient, such as vacuum, is applied, kinematic and frictional coupling increase, resulting in dramatically altered mechanical properties. Engineers have used jamming to build devices from tunable-stiffness grippers to tunable-damping landing gear. This study presents a rigorous framework that systematically guides the design of jamming structures for target applications. The force-deflection behavior of major types of jamming structures (i.e., grain, fiber, and layer) in fundamental loading conditions (e.g., tension, shear, and bending) is compared. High-performing pairs (e.g., grains in compression, layers in shear, and bending) are identified. Parameters that go into designing, fabricating, and actuating a jamming structure (e.g., scale, material, geometry, and actuator) are described, along with their effects on functional metrics. Two key methods to expand on the design space of jamming structures are introduced: using structural design to achieve effective tunable-impedance behavior in specific loading directions, and creating hybrid jamming structures to utilize the advantages of different types of jamming. Collectively, this study elaborates and extends the jamming design space, providing a conceptual modeling framework for jamming-based structures.

1. Introduction

Structures with the ability to actively control stiffness and damping allow for adaptable and versatile interactions between machines and their environments. Precision, high forces, and speed are made possible with high stiffness. Conformability, adaptability, and safe interactions, on the other hand, are made possible with low stiffness. Variable damping allows structures to respond to varying external disturbances in unpredictable environments and allows a tunable frequency response. There are many kinds of variable impedance actuators and structures such as systems with antagonistic actuation, low melting point alloys, shape memory polymers, magnetorheological or electrorheological fluids, and dielectric elastomers. Methods range from changing the impedance only through control, to changing the stiffness and damping at a material level. One mechanism that allows for tunable mechanical impedance at a structural level is jamming. Jamming structures have been particularly attractive since, compared to the abovementioned variable stiffness mechanisms, they are easily scalable, easy-to-fabricate, low-cost, relatively agnostic to material, and can be actuated using a wide variety of mechanisms. They are also able to provide orders of magnitude changes in stiffness, which can be tuned by altering the structures' geometric properties.[1–6]

A jamming structure typically consists of a collection of elements that has a low overall stiffness and damping. Once a pressure gradient is applied to the structure, such as by placing the elements in an airtight bag and applying a vacuum, the kinematic and frictional coupling between the elements increase, resulting in dramatically altered mechanical properties. Elements of varying geometries have been used in jamming structures, namely grains, fibers, and layers.[7–10] The different kinds of jamming structures and their ability to provide tunable stiffness and damping have been of interest to engineers, designers, and roboticists for many different applications, including but not limited to grippers, soft robot locomotion, haptic interfaces, manipulators, surgical robots, deformable furniture, wearable robots, and soft damping mechanisms[11–19] (**Figure 1**).

Roboticists, engineers, and physicists have been working on not only utilizing the capabilities of jamming structures, but also characterizing and predicting their behavior through experiments and modeling. These have provided great insights on application, geometry, and scale-specific behavior of jamming structures.[10,20–26] There have been a few studies comparing the performance of structures with different constituent geometries (e.g., layers and grains) as well, but these studies have been limited to specific applications.[6,27–29] Thus far, there has not been a global and systematic approach to the design space of jamming for target applications.

This study begins with a global comparative analysis of jamming structures' fundamental mechanical behavior, focusing on the deformation modes under different loading conditions. The analysis allows engineers to compare the qualitative mechanical behavior of jamming structures with different constituent materials. The analysis is followed by a list of major design parameters that go into fabricating a jamming structure, such as the scale of constituents, the material choice, and the actuation method. These parameters

B. Aktaş, Dr. N. Vasios, Prof. K. Bertoldi, Prof. R. D. Howe
Paulson School of Engineering and Applied Sciences
Harvard University
Cambridge, MA 02138, USA
E-mail: howe@seas.harvard.edu

B. Aktaş, Dr. N. Vasios, Prof. K. Bertoldi, Prof. R. D. Howe
Wyss Institute for Biologically Inspired Engineering
Boston, MA 02138, USA

Dr. Y. S. Narang
NVIDIA Corporation
Seattle, WA 98052, USA

The ORCID identification number(s) for the author(s) of this article can be found under https://doi.org/10.1002/adfm.202007554.

DOI: 10.1002/adfm.202007554

 © 2021 Wiley-VCH GmbH

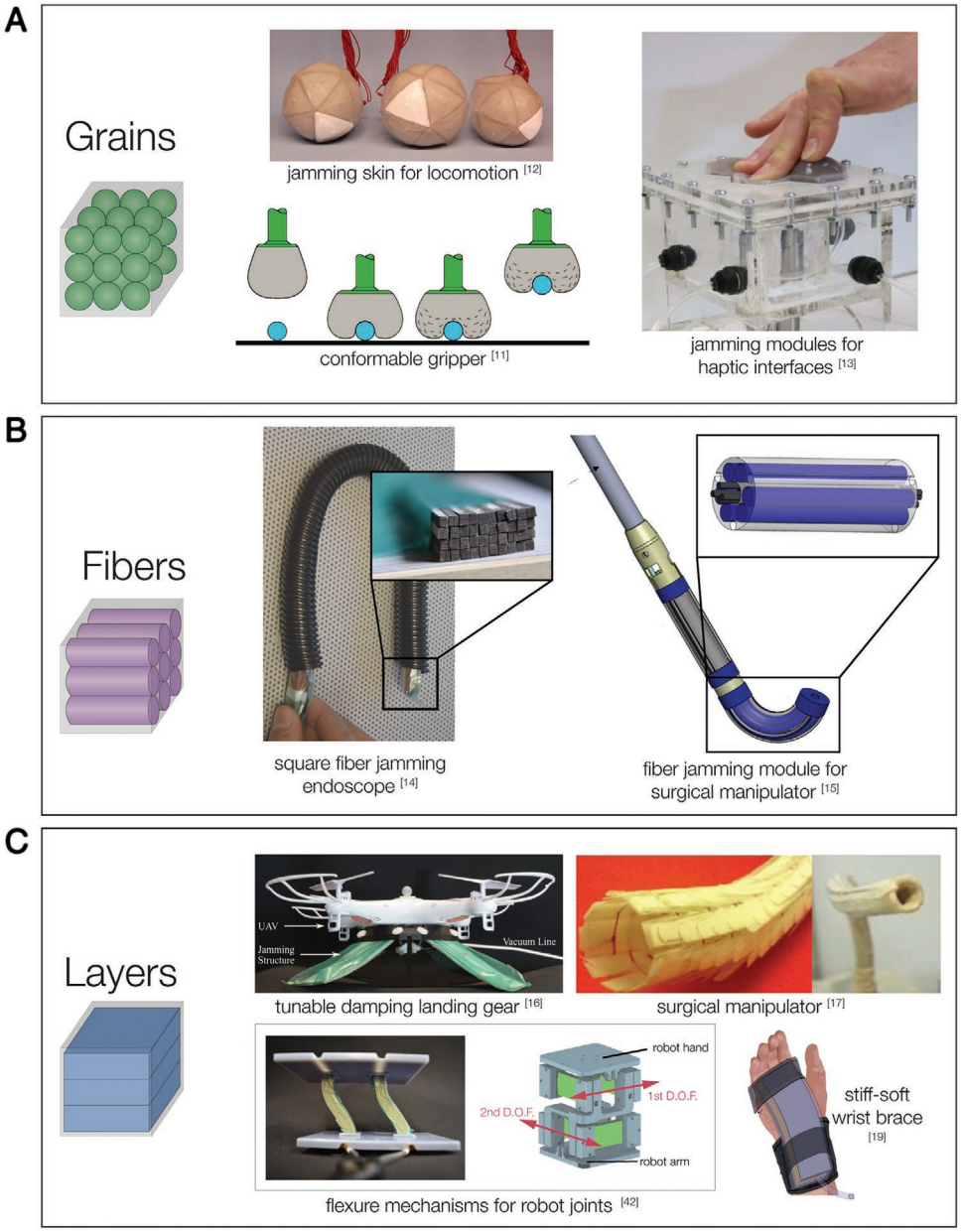

Figure 1. Leading applications of jamming from the literature. A) Granular jamming, with its conformability and isotropic tunable stiffness, has been used for locomotion, grasping, and haptic interactions. (Image copyright information, from left to right: Reproduced with permission.[11] Copyright 2010, National Academy of Sciences. Reproduced with permission.[12] Copyright 2009, IEEE. Reproduced with permission.[13] Copyright 2013, IEEE). B) Fiber jamming, with its ability to provide multidirectional variable bending stiffness in long and slender elements, has been used for medical applications, such as endoscopes and surgical manipulators. (Image copyrights information, from left to right: Adapted with permission.[14] Copyright 2020, IEEE. Adapted under the terms of the CC-BY license.[15] Copyright 2019, Brancadoro, Manti, Grani, Tognarelli, Menciassi and Cianchetti). C) Layer jamming, with its unidirectional variable bending stiffness, has been used for a variety of applications such as landing gear, surgical manipulators, joints for rigid robots, and wearables. (Image copyright information, from left to right. Upper row: Reproduced with permission.[16] Copyright 2017, IEEE. Reproduced with permission.[17] Copyright 2013, IEEE. Lower row: Reproduced with permission.[42] Copyright 2019, IEEE. Reproduced with permission.[19] Copyright 2020, Mary Ann Liebert Inc).

are introduced along with their influence on the structure's performance. The results of the proposed framework are then used to formulate two novel design strategies: first, structural design to exploit specific jamming structures' high performance in particular loading conditions, and second, hybrid jamming, which combines the distinct advantages of different constituent geometries. Altogether, this study provides designers, engineers, and roboticists with tools and guidelines to make design decisions when incorporating jamming into their robotic systems.

 © 2021 Wiley-VCH GmbH

2. Results

2.1. Performance under Fundamental Loading Conditions

Jamming structures and their ability to provide different forms of variable impedance have led to many robotics applications.[7–19,27–51] Yet prior work does not provide a framework to allow engineers and designers to manage performance-based trade-offs when designing jamming structures for applications. In this section, we first outline the fundamental behavior of grains, layers, and fibers as observed in their leading applications in robotics. Then, since the force–displacement behavior is the most critical factor for a variable stiffness and damping element within a robotic system, we develop a set of tools and definitions to connect the mechanical phenomena within a jamming element (namely, the modes of deformation) to its structure-level force–displacement performance.

The concept of jamming was introduced by Liu and Nagel to describe the onset of rigidity in a wide range of systems (including glasses, colloids, and granular materials) comprised of large numbers of constituent elements that interact through short-range, nearest-neighbor forces.[23,24] This concept was later extended to frictional interactions by others.[21,26] In the simplest case, jamming can be described as a phase transition from a state without a yield stress to a state with a yield stress. In the granular matter community, jamming has been analyzed using a phase diagram, in which the three axes are free volume (inverse density), applied shear stress, and temperature.

More recently, especially in robotics, researchers have extended the jamming of granular material to layers and fibers. In these contexts, "jammed" refers to a state when mechanical coupling between constituents (e.g., through application of external pressure) causes a resistance to sliding or rearrangement, rigidity is high, and a yield stress is present. On the other hand, "unjammed" refers to a state when there is a lack of coupling between constituents (e.g., through removal of pressure), rigidity is low, and a yield stress is not present. Critically, the change in mechanical behavior due to the interconstituent coupling cannot be studied independently of the geometry of the constituent elements. The following outline and analysis provide a framework that allows for direct comparisons between the performances of different types of jamming structures with different geometric properties.

Granular jamming, the most widely used and studied kind of jamming, typically consists of granular elements such as coffee grounds, glass, or plastic beads in an airtight bag (**Figure 2**A). When no pressure is applied, the grains move freely with respect to each other, behaving much like a liquid. When a pressure is applied, the grains are constrained, and the structure transitions to a solid-like state. As a result, it is much stiffer and is able to retain its shape. Granular jamming structures which have been integrated into robotics systems have achieved reported stiffness changes of up to 40:1.[3] Beyond this range of performance, granular jamming structures have yielded impressive performance when incorporated into grippers and haptic interfaces, since they are particularly fitting for applications in which conformability and 3D stiffness tunability are important.[11,13,30]

Layer jamming consists of sheets of a compliant material placed in an airtight envelope (Figure 2C). When no is pressure applied, the layers slide freely with respect to one another, having an overall low stiffness. When a pressure is applied, the increased friction causes each layer to couple with the adjacent layers. As a result, the entire structure behaves like one cohesive beam rather than independent discrete layers. The stiffness of the jammed structure is high, until the shear stress induced in the beam is able to exceed the frictional stress caused by the applied actuation pressure. Past that point, the layers begin slipping with respect to each other, and the structure behaves similarly to a Coulomb friction damper. These structures have led to versatile and

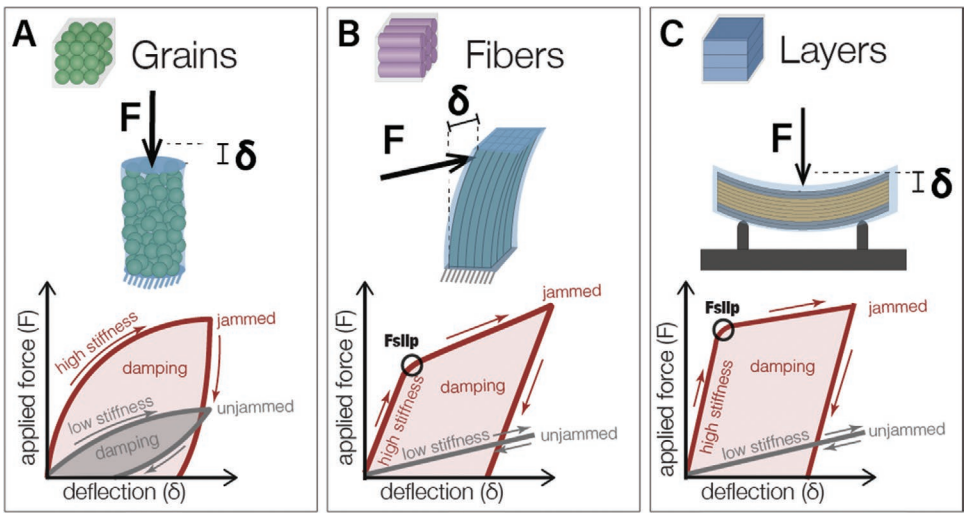

Figure 2. Fundamental mechanical behavior of jamming structures. A) For granular jamming elements under compression, there is a dramatic change in stiffness upon jamming. However, there is no distinct point of slip, and the stiffness is not constant throughout the deflection. Both the jammed and unjammed states have damping, as the deformation is mostly irreversible.[11,40] B) For fiber jamming structures in cantilever bending, there is a distinct point of slip. Before slip, the stiffness is constant and the deformation is elastic. After slip, the stiffness is much lower and constant, but the deflection is irreversible, exhibiting a plastic deformation behavior. When the structure is unjammed, there is effectively no damping and the behavior is purely elastic.[9,14] C) Layer jamming structures in three-point bending also have a distinct point of slip. Before slip begins, there is a constant high stiffness, and after all the layers have slipped, there is a constant low stiffness. The unjammed layer jamming structure also behaves elastically[10,19] (Illustrations depict idealized behavior, based off of prior studies referenced in the caption).

© 2021 Wiley-VCH GmbH

high-performance wearable devices, drone landing gear, and deformable furniture and manipulators, as they have highly-controllable directional stiffness and damping while retaining structural integrity and a low profile.[10] Using layer jamming, roboticists have achieved a bending stiffness change of up to 1800:1.[19]

Fiber jamming, on the other hand, consists of longitudinal fibers in an airtight envelope (Figure 2B). Along one plane, the fibers can rearrange like grains, whereas on the two other orthogonal planes, they slide with respect to each other like layers. These structures have been particularly useful in applications with long and slender elements that need variable bending stiffness in more than one direction, such as endoscopes and surgical manipulators.[9,15,20] With fiber jamming structures, a change in bending stiffness of 5:1 has been achieved.[8]

The fundamental behavior of grain, fiber, and layer jamming, and their diverse application areas demonstrate that each of these structures has unique advantages. More specifically, the behavior of each structure uniquely depends on how it is loaded (e.g., compression vs bending), making it more favorable for certain applications and unfavorable for others. In order to provide a useful design tool, we look at all three kinds of jamming structures under the fundamental loading conditions (tension, compression, shear, bending, and torsion), and determine the modes of deformation for each condition.

We define four fundamental deformation modes which can govern a jamming structure's force–deflection behavior, namely frictional, kinematic, bulk, and actuation. Frictional mode occurs when there are continuous surfaces that are sliding with respect to each other, and the effective stiffness is due to the friction on those surfaces. Kinematic mode occurs when the effective stiffness is a result of the geometric arrangement of the constituents. In the kinematic mode, there may still be friction among the constituents, but frictional interactions are not confined to one surface. In Bulk mode, the structure is completely cohesive in the loaded dimension, and it behaves as if it does not have distinct constituent elements. In Actuation mode, the loading is only pulling the constituents apart, resisted by the actuation forces. The stiffness is only caused by the applied pressure and physical constraints from the actuation method, such as the elastic behavior of the encasing membrane for vacuum-based actuation. Other actuation methods include mechanical coupling, such as meshes, cables and clamps, and electrostatic or magnetic coupling. These four definitions can be used to analyze the jamming behavior of grains, fibers, and layers under fundamental loading conditions, and can then be used to infer their performance in different directions in terms of stiffness tunability. **Figure 3**A shows this analysis, carried out through orthographic projections.

Both bulk and actuation modes lead to ineffective stiffness tunability. Bulk behavior does not have tunability at all, and actuation behavior mostly depends on the force–deflection behavior of the envelope, rather than the constituent media. Since its behavior is more predictable and without slip, the bulk mode might be more favorable along a dimension of a structure that does not need to be tunable. Frictional and kinematic modes, on the other hand, lead to effective stiffness tunability, and they have different force–deflection behaviors.

In the frictional mode, which only occurs under shear, bending, and torsion, there is a distinct point of slip.[10] Before slip, the structures behave as if they are in the bulk mode, deforming as if their constituent layers or fibers are not independent. This cohesion results in a high-stiffness regime in which the force–deflection behavior is consistent with the material's inherent stress–strain behavior. After this point of slip, the layers or fibers start sliding with respect to one another. If in shear, the structure has zero stiffness (Figure 3C). If in bending, it has an overall low stiffness that is equal to the unjammed stiffness, which is the sum of the stiffnesses of the separate layers or fibers (Figure 3D). Since there is frictional sliding in between the layers, there is energy dissipation in the post-slip stage. The overall deformation is irreversible, and the structure behaves similar to a Coulomb friction damper. For layers in torsion, depending on the axis about which torsion is applied, the behavior could exhibit either a post-slip stiffness of zero or have a low stiffness equal to the sum of the stiffnesses of the separate layers.

For the materials considered in this study, the preslip behavior in the frictional mode is largely linear elastic, and the stiffness is governed by the combination of the shear modulus, G, or Young's modulus, E, as well as geometric parameters of the structure. The next three paragraphs look into the modeling of the jammed preslip stiffness and the unjammed stiffness of structures in the frictional mode under shear, bending, and torsion, respectively.

For shear (Figure 3C), the preslip stiffness is $\frac{\partial F}{\partial \delta} = \frac{GA}{H}$, where F is the applied force, δ is the resulting deflection, A is the area across where the shear force is applied, and H is the total height. For a rectangular beam made up of N layers parallel to the neutral surface, with dimensions shown in Figure 3G, the shear stiffness would be equal to $\frac{\partial F}{\partial \delta} = \frac{GbL}{Nh}$, where b is the width and h is the height of each layer. Note that this is the preslip stiffness when the structure is jammed. In the unjammed or post-slip state, the shear stiffness of the jamming structure is effectively zero and is determined by the elasticity of the encasing envelope.

The bending stiffness (Figure 3D), according to Euler Bernoulli beam theory, is $\frac{\partial F}{\partial \delta} \propto EI$, where I is the moment of inertia. For the layer jamming structure shown in Figure 3G, the moment of inertia during the preslip regime would be $I_{\text{preslip}} = \frac{bN^3h^3}{12}$, as the structure behaves like one large cohesive rectangular beam. Note that this is N^2 times larger than the stiffness in the unjammed state, where the layers are freely sliding with respect to each other, and the moment of inertia is only the sum of the independent layers $\left(I_{\text{unjammed}} = \frac{Nbh^3}{12}\right)$. For jamming structures with circular fibers under bending, the theoretical modeling of the bending stiffness is not as trivial, since different packing arrangements are possible.[20] Considering hexagonal packing (shown in Figure 3F), which achieves the highest packing density possible for circles and assumes the gaps between the fibers are negligible, we can estimate the moment of inertia of the resulting hexagon and therefore the change in stiffness upon jamming. If there are N number of fibers each with diameter d, the side dimension of the resulting hexagon will be $a = d\sqrt{\frac{N}{3}}$. The moment of inertia of the hexagonal cross-section will give $I_{\text{preslip}} = \frac{5\sqrt{3}N^2d^4}{144}$. The unjammed stiffness can be determined by summing the moment of inertias of the independent circular fibers $I_{\text{unjammed}} = \frac{\pi N d^4}{64}$.

© 2021 Wiley-VCH GmbH

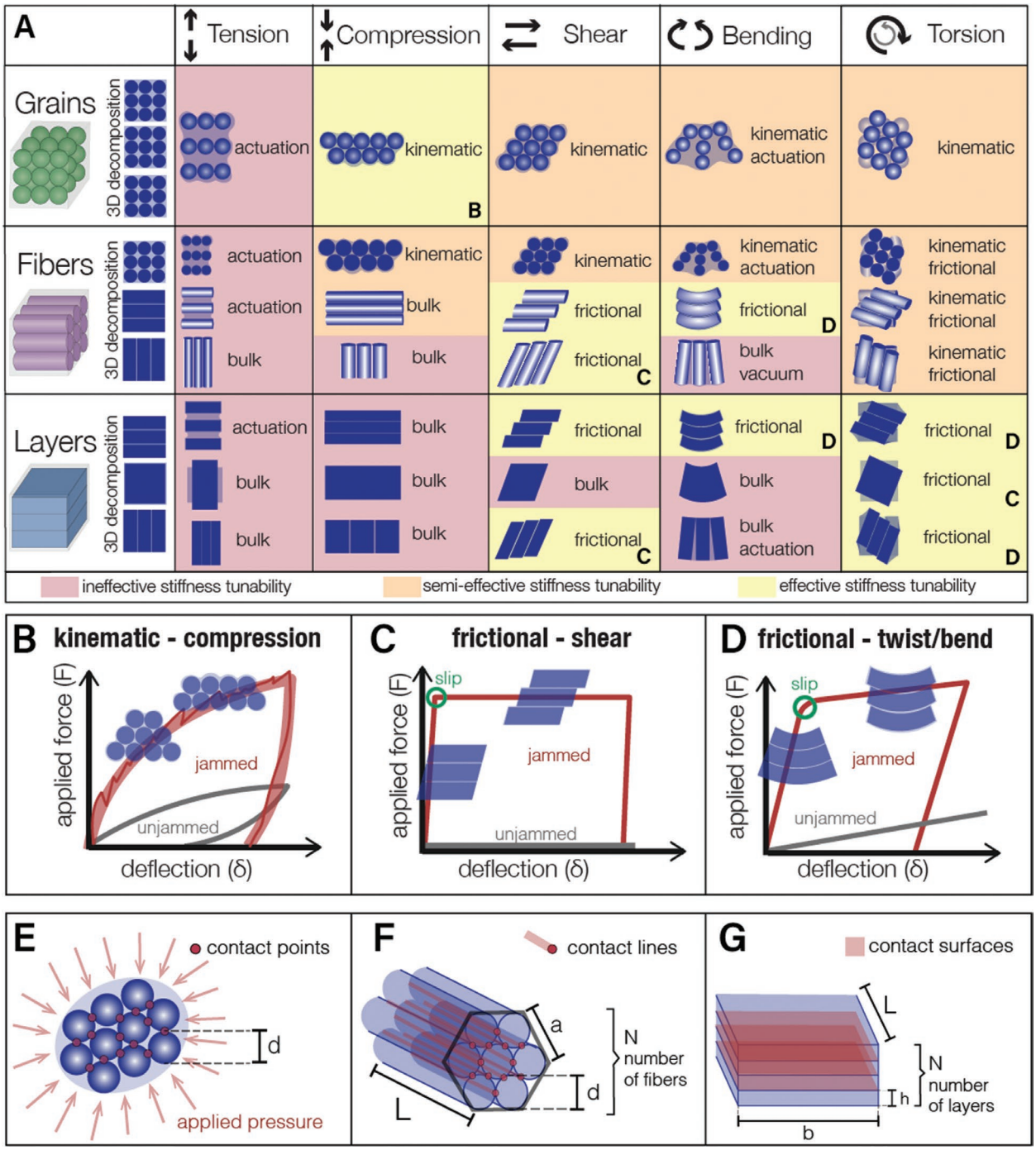

Figure 3. Deformation modes of elementary jamming structures. A) The deformation mode governing the jamming structure for each type of media (grain, layer, and fiber) under each fundamental loading condition is shown (See Video S1, Supporting Information). B) Representative force–deflection curve for the kinematic deformation mode.[11,40] Note that there is typically non-monotonic behavior (shown with the thin dark red line) due to localized geometric rearrangements. C) Representative force–deflection curve for the frictional mode in which the applied force only causes sliding between the constituents.[20,34] D) Representative force–deflection curve for the frictional deformation mode in which there is not only sliding, but also bending and/or twisting.[9,10,14,19] E–G) Contact geometries for jamming structures with grains, fibers, and layers are, respectively, points, lines, and surfaces.

Note that the change in stiffness upon jamming is $N\frac{20}{3\pi\sqrt{3}}$. This is different than the N^2 range of stiffness achieved by layers, since the fibers are stacked in two dimensions, rather than one dimension. Note that an increased number of fibers results in an increased range in bending stiffness in all directions, rather than just one. As a result, fiber jamming structures are more fitting for applications where tunable bending stiffness

© 2021 Wiley-VCH GmbH

is required in multiple directions. On the other hand, if tunable bending stiffness in only one direction is desired, a layer jamming structure might be more fitting. Layer jamming structures can be more straightforward to model, and they also exhibit more repeatable behavior due to their stable contact surfaces, compared to the less stable contact lines between circular fibers (Figure 3F,G). In any case, the preceding theoretical modeling based on effective moments of inertia can be used to predict the bending stiffness change that can be achieved by both fiber and layer jamming structures.

Torsional stiffness can be defined as $\frac{\partial T}{\partial \phi} \propto GJ$, where T is the applied torque, ϕ is the resulting twist angle, G is the shear modulus of the material, and J is the polar moment of inertia. For the layer jamming structure shown in Figure 3G, the polar moment of inertia can be approximated as $J_{\text{preslip}} = \beta_{\text{cohesive}} bN^3h^3$, where β is an empirically determined value dependent on the aspect ratio $\frac{b}{Nh}$. Note that this is $\frac{\beta_{\text{cohesive}}}{\beta_{\text{layer}}} N^2$ times the unjammed torsional stiffness where the layers are freely sliding with respect to each other, and the polar moment of inertia is only the sum of the independent layers ($J_{\text{unjammed}} = \beta_{\text{layer}} bNh^3$ where β_{layer} depends on the aspect ratio $\frac{b}{h}$). β_{layer} will always be larger than β_{cohesive}, so the stiffening ratio will be less than N^2. For jamming structures under torsion about the axis perpendicular to the contact surfaces, the preslip stiffness will be equal to bulk torsional stiffness GJ when jammed, where J is calculated based on the geometry in that cross section. The unjammed stiffness will simply be zero, showing a force–deflection behavior as demonstrated in Figure 3C.

For shear, bending, and torsion in the frictional mode, the shear stress at which slip occurs is $\tau_{\text{slip}} = \mu P$, where μ is the coefficient of friction, and P is the applied pressure (Figure 3C,D). To find the applied force which will lead to slip, the maximum shear stress induced should be calculated based on the magnitude and direction of the applied force, as well as the geometry of the sample. For a structure under pure shear, this is simply $\tau_{\max} = \frac{V}{A}$, where V is the total shear force and A is the cross-sectional area, since the shear is distributed equally in the sample. For a rectangular cross section in bending, the maximum shear would occur on the neutral axis, with the value $\tau_{\max} = \frac{3V}{2A}$, where V is the internal shear force and A is the cross-sectional area.[9] For a circular cross section in torsion, the maximum shear would occur on the periphery of the circle, with the value $\tau_{\max} = \frac{Tr}{J}$, where r is the radius.[52] Once the induced maximum shear stress exceeds the shear stress required for slip, the structure enters the post-slip regime. The ability to predict the slip point of a jamming structure is critical for using jamming structures deforming in the frictional mode. Certain applications might require avoiding yield in the structure and staying within the elastic high-stiffness preslip regime, whereas other applications might benefit from a deliberate force threshold that can be implemented through inducing slip. In addition, not only does the slip point allow for a programmable force threshold, it also determines the onset of frictional sliding, which results in energy dissipation. The slip point, which is tunable with the applied pressure, can be used in jamming structures to tune damping capabilities in real time.

In the kinematic mode, the geometric rearrangement of the grains or fibers dominates the deformation. For almost all practical jamming structures, in which the scale of the constituents is much smaller than the scale of the overall structure and the elasticity of the individual elements is negligible, the kinematic mode results in immediate rearrangement. There is no distinct point of slip, as rearrangements occur throughout the deformation regime. As a result, the stiffness is not constant (Figure 3B). A large part of the deformation is not recoverable, as the structure settles into new favorable arrangements under the applied pressure and applied force. The deformation could be elastic either with grains with low elastic modulus (e.g., foam), or when the structure-level deformations are so small that the grains or fibers cannot achieve a new favorable state upon rearrangement, snapping back to their original arrangement upon unloading.[22–26] These instances of elastic deformation in the kinematic mode are not relevant for a large variety of jamming structures used in robotics applications and are thus not considered in detail here.

Providing closed-form theoretical predictions of the mechanical behavior in the kinematic mode is a non-trivial task, and the complexity of behavior can be seen by looking at the vast physics literature on granular matter. However, there are some scaling relations which can inform design decisions. Two major factors influence the stiffness: the packing density and the applied pressure. The packing density is the fraction of volume filled by grains or fibers. An increase in packing density, ϕ, causes an increase in the average number of contact points or lines per element, z, which are shown in Figure 3E,F. There is a critical value of ϕ which is required to achieve enough contact points (z_c) in order for the system to be considered kinematically constrained and "jammed." The effective shear modulus of a jamming structure is proportional to the excess contact number, $G_{\text{effective}} \propto \Delta z$, where $\Delta z = z - z_c$. The relationship between the excess contact points and excess packing density is $\Delta z \approx \Delta\phi^{0.50 \pm 0.03}$. The shear modulus and bulk modulus K are also dependent on the contact stiffness between each particle, which is determined largely by the applied pressure P. The scaling relationship is the same for both effective elastic moduli, with $G_{\text{effective}} \propto P^{1/3}$ and $K_{\text{effective}} \propto P^{1/3}$.[26] These scaling relationships provide insights on how the phenomena governing the interactions between the constituent elements impact the mechanical behavior of the overall jamming structure.

Fibers under torsion exhibit complicated mechanical behavior that is a combination of kinematic and frictional deformation modes. Throughout deformation, the contact lines between the fibers transition into contact points after slip occurs. The arrangement of the fibers is crucial for determining the mechanical behavior. For example, if a square arrangement of fibers undergoes torsion about an axis orthogonal to the fibers' length, the structure will begin deforming in a frictional mode. The preslip torsional stiffness will be equal to the bulk stiffness, calculated through GJ. Once slip occurs

© 2021 Wiley-VCH GmbH

at a point along a contact line, the kinematic deformation mode will dominate. For any other arrangement, it is difficult to gauge which deformation mode will dominate and whether or not there will be a distinct point of slip. If torsion is applied about an axis along the length of the fibers with a hexagonal arrangement, as shown in Figure 3F, it is also difficult to gauge whether or not there will be a distinct point of slip. However, we can calculate the upper and lower bounds for the torsional stiffness. The upper bound will be the stiffness of the cohesive hexagonal beam, determined by the polar moment of inertia $J_{\max} = \frac{5\sqrt{3}}{72} N^2 d^4$. The lower bound of the stiffness can be calculated by summing the torsional stiffnesses of each separate fiber. This is an approximation, as only the central fiber will undergo pure torsion; all surrounding fibers will also experience bending, morphing from straight lines into helices. Since the torsional stiffness will be much larger than the bending stiffness, only considering the torsional stiffness of each fiber results in $J_{\min} = \frac{\pi}{2} N d^4$. These maximum and minimum values can serve as a guideline to get a sense of the performance; however, it is important to note that the behavior of fibers in torsion is still an open research question that requires further investigation via theory, simulation, and experiments.

In order to clearly visualize and identify the deformation modes, the analysis shown in Figure 3A has specifically looked at in-plane deformations through orthographic projections. It is important to note that, in order to predict the 3D behavior of a jamming structure using Figure 3A, the loadings and deformations in multiple planes have to be considered. For example, when considering fibers under compression along a direction that is orthogonal to the length of the fibers, one plane will exhibit bulk behavior while the other will exhibit kinematic behavior. In this case, unless the fibers are unable to rearrange due to external constraints, the kinematic behavior will dominate, since it allows for a lower-energy shape transformation. On the other hand, when considering a granular jamming structure under compression, we see that all dimensions allow for kinematic rearrangement. As a result, compared to fibers in which the kinematic rearrangement is constrained to one plane, the grains can rearrange in any direction. A greater number of contact points leads to a greater stiffness and damping difference between the jammed and the unjammed state.

The above analysis provides a tool to not only predict the mechanical performance of different constituent element geometries, but also to guide the design of a jamming structure for a specific application. For example, an application might require a variable-stiffness leaf spring, and thus requires an elastic-stiff and an elastic-soft state in bending in one specific direction. Elastic deformation in both the jammed and unjammed states can only occur in the frictional deformation mode, so the constituent geometry can either be layers or fibers. Since the bending is only occurring in a single direction, we can use layers, as long as we make sure the neutral surface of bending is parallel to the contact surface between the layers. Layers are also preferable to fibers in order to avoid the effect of off-axis loading, which might cause irreversible deformation due to kinematic behavior.

Overall, the analysis constructed in this section provides a toolkit to interpret and predict the multidirectional force–deflection behavior of jamming structures. It facilitates informed decisions for constituent geometry, and also provides guidelines on how to align and position the jamming structures with respect to the loading conditions.

2.2. Design Parameters

Designing a jamming structure for a particular application requires more than deciding on the constituent geometry (grain, fiber, and layer). The constituent geometry, as explained in the previous subsection, will only determine the fundamental mechanical behavior. Other design parameters such as the scale of constituents, the material choice, and actuation method have a great influence on both the structure's performance and its appropriateness for integration with an existing system. This section serves as a checklist of major decisions that need to be made when designing and fabricating a jamming structure for a particular purpose. A list of major design parameters is provided, along with the influence of each parameter on structural performance. **Figure 4** demonstrates examples of decisions that could be made with regards to each of these parameters.

2.2.1. Constituent Geometry

Other than the simple geometries mentioned above (layers, fibers and grains), more complex morphologies can also be designed in order to create precise deformation modes in specified directions. Interlocking geometries can be utilized to create kinematic constraints to only allow for motion in particular directions.[31–35,53–57] Fibers can have prismatic cross sections, rather than circular ones to avoid kinematic rearrangement in particular directions and to transform the contact lines between constituents into contact surfaces.[14] Particles can be designed with particular geometries to create larger number of contact points, or larger contact surface areas between the particles.[6,36] Micromachining the surfaces of constituents can allow for a wider range of friction coefficients.[37] Figure 4A shows some possible constituent geometries that have been used in literature. Different constituent geometries can also be combined within a single jamming structure to utilize the advantages of the different geometries. An example of a hybrid jamming structure which uses both layers and grains is provided in the subsection below.

2.2.2. Material

The material choice for the constituents influences the mechanical performance due to material-specific stress–strain behaviors and friction coefficients. The elastic modulus of a material influences the minimum and maximum values the stiffness can reach, particularly when the structure is deforming under the frictional mode. The friction coefficient influences the slip behavior: smaller values will result in the constituents sliding with respect to one another under smaller loads. The impact

© 2021 Wiley-VCH GmbH

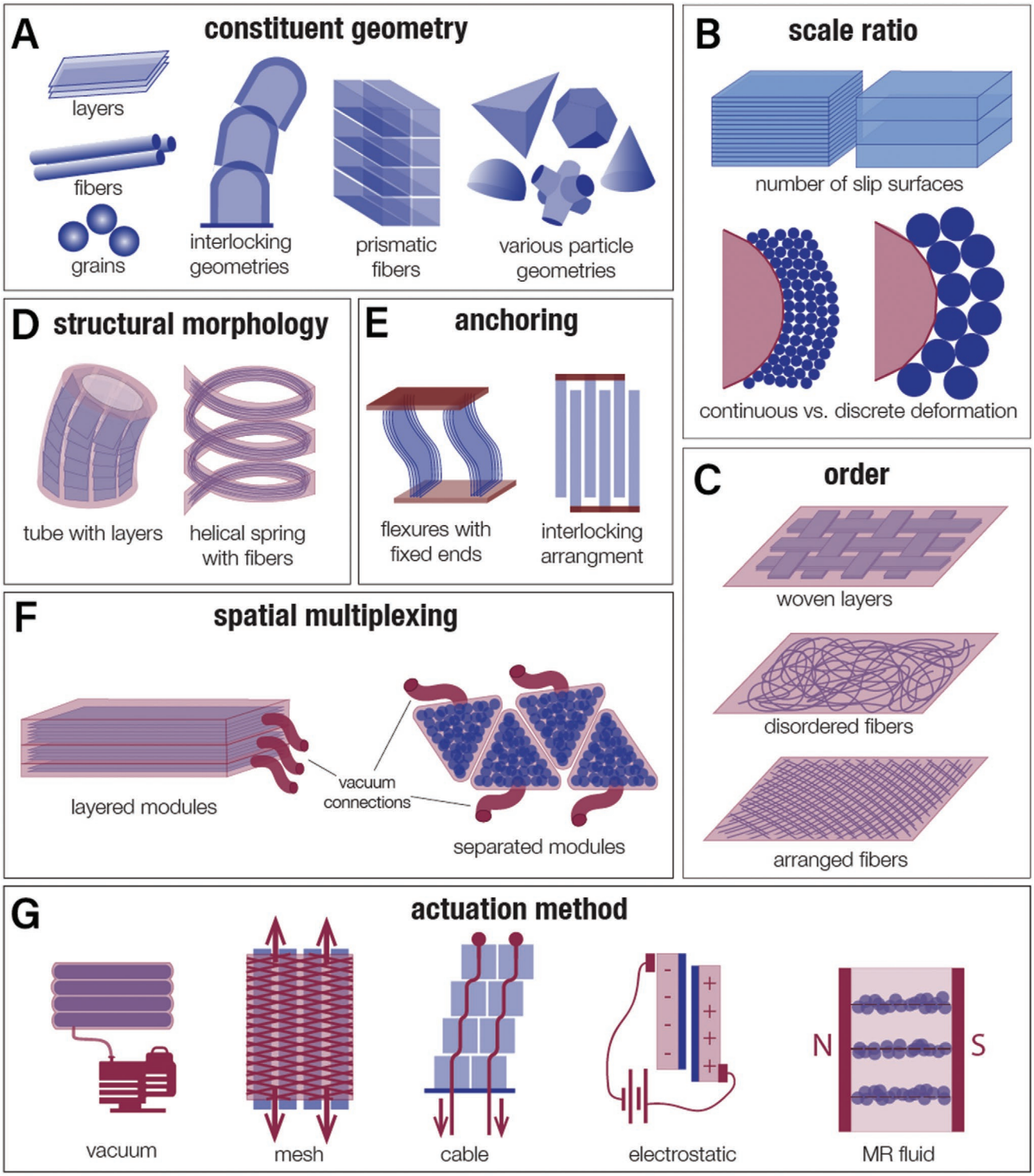

Figure 4. Design parameters of a jamming structure. A) Other than layers, fibers, and grains, various constituent geometries can be used to achieve particular mechanical behavior through kinematic constraints. B) The scale ratio between the constituents and the overall structure impacts both the amount of slip surfaces/lines/points and the way the structure interacts with the scale of application. C) Constituents can be ordered in varied ways within a structure, to achieve specific anisotropic/isotropic mechanical behavior. D) The geometry of the overall structure can be used to utilize the high-performing deformation modes of each structure to achieve variable stiffness in the direction of motion. E) The constituents can be anchored to a system in specific ways, taking advantage of a deformation mode in a particular direction. F) Multiple airtight envelopes can be brought together to create modules in order to tune the stiffness with higher precision or to separately stiffen and soften different segments of a structure. G) Other than vacuum, mechanical meshes and cables, electrostatic coupling, and magnetorheological fluids can also be used to induce jamming behavior.

 © 2021 Wiley-VCH GmbH

of material properties on the performance of jamming structures have been analyzed through experimental studies and modeling.[10,38,39] There have also been studies demonstrating the advantages of combining different materials. One strategy is including separate constituents made of separate materials within a single structure. An example is sandwich layer jamming structures, where high-stiffness face layers and low-density core layers are combined to substantially improve stiffness-per-weight performance.[19] Another strategy involves creating specialized composite materials for the constituents. For example, plastic grains can be coated with a layer of rubber, resulting in grains with both high stiffness and high surface friction.[40]

2.2.3. Scale Ratio

The size of the constituent elements, compared to the size of the overall structure and the application, influences the jamming behavior by changing the number of contact and slip points in the entire structure (recall Figure 3E–G). Smaller constituents within a given volume results in a higher range of mechanical impedance, that is, a larger difference in stiffness and damping between the jammed and unjammed states. Particularly in conditions where the kinematic mode of deformation is prevalent, smaller particles lead to more continuous deformations, whereas larger particles result in more discrete deformations. As a result, smaller particles also allow for more conformability compared to larger ones (Figure 4B).[10,14,58]

2.2.4. Order

The elements within a jamming structure can be ordered in non-uniform ways in order to create tunable anisotropy, as demonstrated in Figure 4C. Fibers can be oriented in two orthogonal directions or can be completely disordered, and layers can be woven.[18,27,59,60] An important consideration is the retention of the prescribed order throughout applied deformations and loadings, and the impact of disarrangements on the overall performance of the structure. For example, for woven fibers, the position of the fibers with respect to each other might remain fairly fixed, yet any disarrangement might significantly alter the desired anisotropic behavior. On the other hand, while disordered fibers might be more prone to disarrangements, the disorder might not cause significant deviations from the desired performance. The impact of the disarrangement of the constituents on the reliability of the structure, which occurs especially when kinematic deformation modes are prevalent, can be minimized by having the scale of the constituents much smaller than the scale of the structure.

2.2.5. Structural Morphology

The geometry of the overall jamming structure governs the relationship between the global loading condition (determined by the interaction between the structure and the environment) and the local loading condition (determined by the resulting induced load on the jamming constituent level). Existing means to optimize overall structural geometry can be used to achieve specific elastic behaviors for jamming structures; for example, construction of leaf springs, helical springs, tubular structures, and flexures.[17,42] Granular jamming structures' high performance in compression can be utilized in bending by creating off-center granular jamming pillars.[43] Layer jamming structures can be folded into origami-inspired mechanisms.[44] Some of these possibilities are shown in Figure 4D. A novel example of using structural design to achieve loading specific tunable elastic behavior is included in the following subsection.

2.2.6. Anchoring

A jamming structure can be anchored to a system in a large variety of ways. The analysis in Section 2.1 focused on the localized behavior within a unit cube of a structure, yet the different types of anchoring can allow for different deformation modes by creating boundary conditions that prompt specific sliding processes and stress/strain distributions. One commonly utilized anchoring method is mounting alternating fibers/layers to the two different ends of the structure (Figure 4E). When these structures are under tension, and the comb-like interfaces are pulled apart, the deformation mode is frictional. The structure is effectively a frictional clutch, and the force–deflection behavior is similar to Figure 3C.[34,49,61,62] Another example of anchoring is when both ends of a layer jamming structure are clamped. These boundary conditions cause the structure to behave like a parallel leaf spring, with only a single degree of freedom. This can be utilized to create jamming-based flexures that have variable stiffness along specific degrees of freedom.[42]

2.2.7. Spatial Multiplexing

A structure can have separate segments that are jammed and unjammed independently, which can be achieved through fabricating disconnected airtight envelopes that are connected to separate valves. This allows for multistate modular systems, which can be used to create structures with separately controllable localized stiffnesses.[12,13,45] Another advantage, specifically for structures deforming under the frictional mode, is the ability to achieve multiple stiffness values. In the frictional mode, the applied pressure only changes the point of slip; the preslip and post-slip stiffnesses remains constant, resulting in a binary stiffness behavior. Layering multiple structures and connecting them to separate actuation sources allow the compound structure to achieve a larger variety of stiffness values (Figure 4F).[10]

2.2.8. Actuation Method

The chosen actuation method, which could be pneumatic (vacuum or positive pressure), mechanical (clamps, meshes, and tendons), electrostatic, or magnetic, introduces opportunities and limitations. Vacuum is convenient since it can achieve consistent isotropic pressure throughout a jamming structure,

© 2021 Wiley-VCH GmbH

and the fabrication processes are easily scalable. Yet it requires an external membrane, which can create design complications for system integration. The material of the membrane also can have a significant influence on a jamming structure's performance.[40,63] A vacuum-actuated jamming structure has an upper bound on the vacuum pressure within the enclosing structure (i.e., when a perfect vacuum is achieved). This limit, which will result in an applied pressure equal to the atmospheric pressure, restricts the range of slip thresholds a structure can achieve. Mechanical actuation methods allow for directional control of the applied pressure; for example, if there are clamps that operate in orthogonal directions, two directions can be separately jammed or unjammed. There is no fundamental physical upper bound for the applied pressure in mechanical methods. They also introduce the need for mechanical actuators, which may or may not be favorable compared to pneumatic pumps for a given application.[31,46–48,64] Electrostatic or magnetic methods of jamming also have the advantage of providing directional pressures with high magnitudes.[49,50,61,62] One limitation is volume, since unlike mechanical clamps or vacuum, the applied pressure will decrease as the distance between the two charged surfaces increases. Another limitation of electrostatics is the requirement of high voltages, which might limit applications with safety concerns. These different actuation methods could also be combined in order to achieve the desired performance. For example, a pneumatic jamming approach can be implemented, but the pneumatic valves within a system can be operated using electrical charge.[51]

2.3. Structural Design: Leveraging Directional Behavior

Understanding the directional performance of jamming structures under different loading conditions enables the use of the best performing deformation modes for specific applications through structural design. Given a particular loading condition prescribed by a specific application, the geometry of the jamming structure can be designed such that the loading on the local level (i.e., on the jamming constituent level) corresponds to the high-performing loading condition for that particular type of jamming element. Through a case study, we demonstrate how to use structural design to exploit the directional behavior of jamming structures.

As seen in Figure 3, none of the elementary jamming structures perform well under tension. As mentioned in Section 2.2.6, there have been jamming structures with interlocking arrangements that work in tension. These only allow for a stiffness that can alternate between the shear modulus of the material and zero. The low- and high-stiffness values cannot be programmed by modifying the geometry of the structure. This gap in performance is addressed here by designing a planar spring using layer jamming elements. This planar spring allows for tunable stiffness not only in tension, but also in compression as well as rotation. The geometry is designed such that (Section 2.2.5) the applied load on the overall structure (tension, compression, and rotation) translates to a favorable local loading condition on the local jamming element level (**Figure 5**A). As shown in the analysis in Section 2.1, layer jamming structures demonstrate effective performance both in torsion and bending (Figure 3A). The frictional deformation mode allows for discrete high and low stiffness values (Figure 3D), and results in a jamming structure with jammed and unjammed stiffnesses that can be tuned not only by changing the material, but also by altering the geometry of the structure and the number of layers.

The experimental performance of the planar spring shown in Figure 5C demonstrates that there is an eightfold improvement in stiffness in both compression and tension, and a fourfold improvement in stiffness in rotation upon jamming. The behavior is repeatable across trials and in all the different directions. This tunable-stiffness planar spring and its derivatives can be used to increase the versatility of constant-stiffness planar springs that have been used in applications such as pneumatic valves, bolt assemblies, electrical contacts, and positioning systems.[65] Note that the stiffness range as well as the point of yield can be programmed by altering the dimensions, the number of layers, and the applied pressure.

The resulting spring that has variable stiffness in tension, compression, and rotation shows how the performance space of jamming structures can be expanded by utilizing structural design principles that consider the high-performing deformation modes of jamming structures. This case utilized the high performance of layer jamming elements in bending and torsion. Furthermore, once the major design decisions with regards to constituent geometry and structural morphology allow for the desired behavior, the performance range can then be further expanded by modifying the dimensions, number of layers, and applied pressure (Figure 4).

2.4. Hybrid Jamming Structures: Combining Advantages of Multiple Media

When creating a new jamming structure for a particular application and managing design trade-offs, a single medium (grain, fiber, and layer) might not suffice. Hybrid jamming structures can address this performance gap by combining the unique advantages of different media. Specifically, if an application has two design criteria, each exclusively fulfilled by a different medium, those two kinds of jamming structures may be combined to achieve the required compound performance. We demonstrate how to design hybrid jamming structures to effectively combine the advantages of two different media through a case study.

This example focuses on creating a reusable sleeve for rapid mold-making, a method that can be used to reproduce soft robotic components. A molding sleeve entails several performance characteristics: high-resolution conformability to achieve detail, structural integrity that has elastic behavior in order to retain the overall shape during the removal of the object, and finally, the ability to reset the deformation in order to reuse the same sleeve for molding another object. The reusability specification is met by any jamming structure, since the stiffness change in jamming is typically fully reversible. Granular jamming provides the best conformability, since it exhibits the kinematic deformation mode under the major different loading conditions the structure will experience as it is fitted onto on object, namely compression, shear, and bending (Figure 3A). As a result, granular jamming is a highly suitable

© 2021 Wiley-VCH GmbH

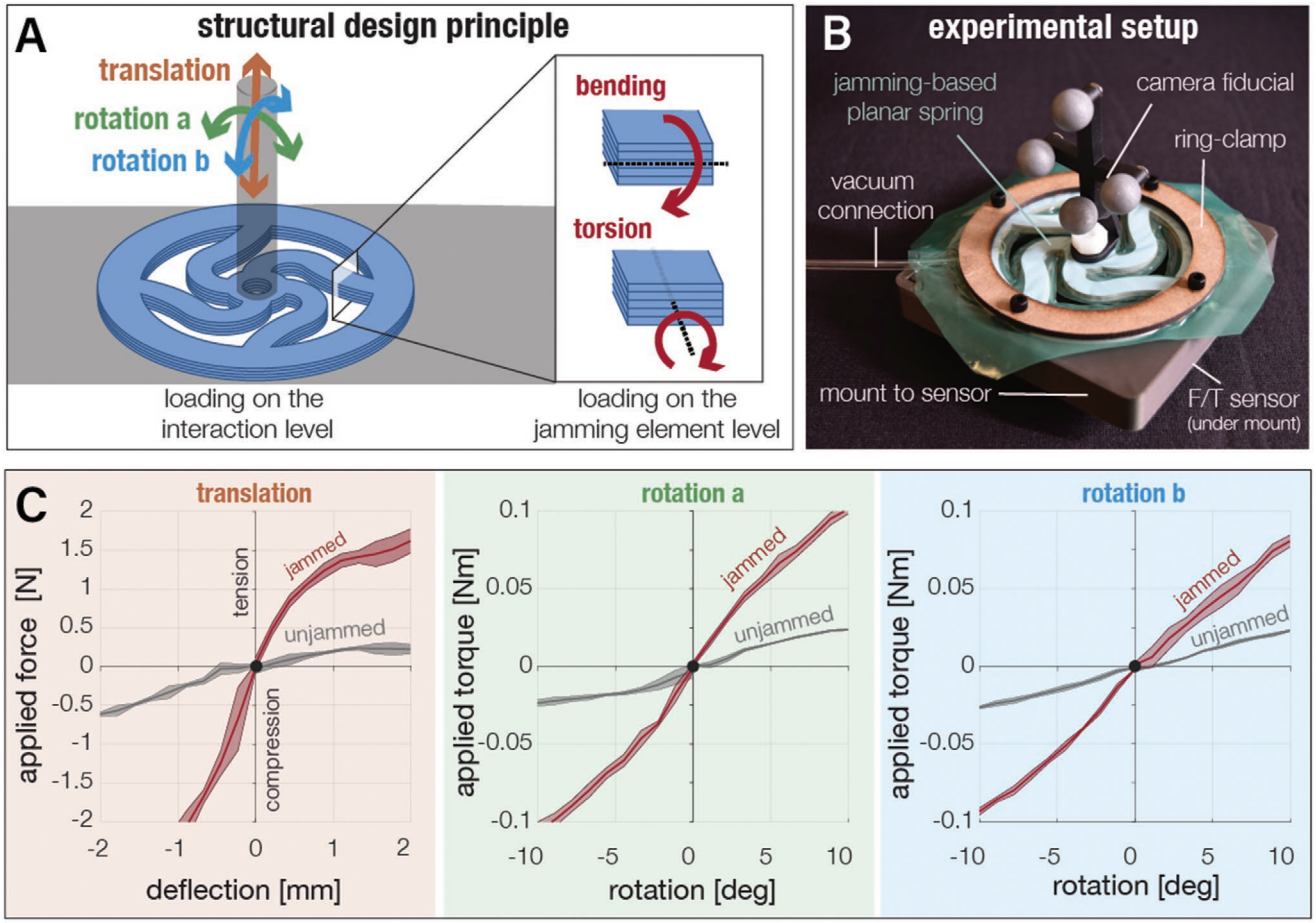

Figure 5. Jamming-based planar spring using structural design. A) The translation and rotations on the global level of the spring lead to bending and torsion on the local level of the jamming structure, allowing the exploitation of the high performance of layer jamming structures under these two loading conditions. B) Experimental setup to collect 3D force displacement data from the planar spring. C) Resulting force–deflection and torque–rotation behavior. Each curve is the average of four trials, and the shaded bar shows the standard deviation.

medium for a mold-making sleeve. However, since the only deformation mode it has is kinematic, the majority of the deformation is not recoverable. Thus, a pure granular jamming sleeve will not retain its overall shape when it is peeled away from the object. Layer jamming, on the other hand, can provide an elastic spring-back behavior when it is under bending in the jammed state, since it exhibits frictional behavior that allows for a distinct elastic preslip regime (Figure 3D).

In order to empirically validate this comparison and demonstrate the advantage of the hybrid jamming structure, three jamming-based mold-making sleeves are fabricated: one with just layers, one with just grains, and one that is a layer–grain hybrid jamming structure. Each sleeve is used to mold and cast the same object, in this case a squash, and the resulting casts are shown in **Figure 6**. The performances of these three molding sleeves are compared based on their accuracy in replicating the original object as measured by 3D scans. The point-by-point error and the overall root mean square error is shown in Figure 6, alongside superimposed images of the casts' scans and the original object.

The layer-jamming-based molding sleeve retains the overall shape when the object is removed, yet it is not able to preserve any surface detail. The granular-jamming-based molding sleeve is able to preserve the surface detail, but is not able to retain its structural integrity to preserve the overall shape. The layer–grain hybrid molding sleeve, on the other hand, achieves both local detail and global shape. This comparison demonstrates that we can use hybrid jamming as a strategy to achieve two seemingly disparate performance criteria that could formerly only be achieved with different jamming structures.

3. Conclusion

This paper has provided a comprehensive study of the design space of jamming structures, bringing together work from different communities (e.g., mechanics, robotics, physics, and material science). Starting with a comparative analysis of the loading performance of jamming structures with different elementary constituent elements (i.e., layers, fibers, and grains), the study provides guidelines to design and model jamming structures for applications with specific stiffness-tunability needs. The study then proposes two methodologies for extending the range of jamming applications, structural design,

© 2021 Wiley-VCH GmbH

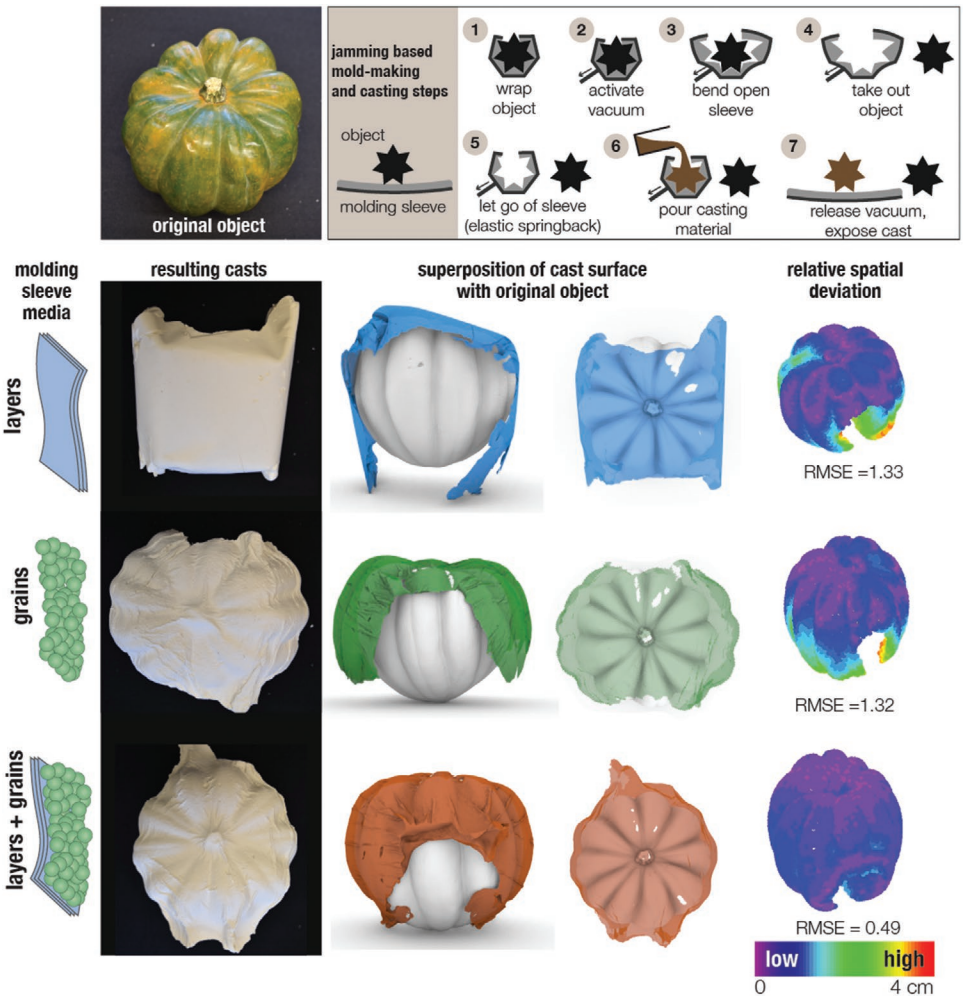

Figure 6. Jamming-based reusable molding sleeve using hybrid jamming. The top panel shows the steps to making a cast using the mold-making sleeve. The resulting casts are presented both as photographs and as renders from high-resolution 3D scans. The color map on the right shows the relative spatial deviation per point, mapped onto the original object.

and hybrid jamming. Both these methodologies, which use the preceding analysis, are then realized with two application-based case studies: a tunable-stiffness planar spring and a reusable molding sleeve. Altogether, this study provides a framework for understanding the design space of jamming structures and offers strategies that expand the design space, facilitating the design of novel high-performing jamming structures for diverse applications.

Figure 7 shows a summary of the functional metrics that have been analyzed in this study: stiffness tunability in the five primary loading conditions, conformability, disarrangement (the degree to which the constituents can spontaneously rearrange within the structure), damping, plastic, and elastic mechanical behavior. This spider plot can be used to immediately see which jamming medium, if any one in particular, can fulfill the needs of a target application.

In cases where a solution is not provided by an elementary jamming structure, the two design strategies described above can be utilized. In this study, the jamming-based planar spring utilized structural design to expand the performance space of layer jamming structures, resulting in a device that can provide effective tunable impedance in both tension and compression. As shown in Figure 7, this was not possible with any elementary jamming structure made of a single medium. The mold-making sleeve, on the other hand, utilized hybrid jamming in order to combine the advantages of two different media: the conformability of granular jamming and the elastic spring-back behavior of layer jamming. As Figure 7 demonstrates, both these case studies expand the design space of jamming and demonstrate that new performance specifications can be achieved through the proposed strategies.

Both design strategies could be used to create other high-performance variable impedance structures. For example, tunable impedance in both tension and compression could be also achieved through helical springs, since the tension and compression of the overall spring would cause bending and torsion along the length of the material. These helical springs could be fabricated with either fibers or layers. In addition, creating a variable-stiffness bending element that does not have elastic ringing behavior upon impact could be achieved by combining the bending performance of fibers and the continuous damping of grains. The resulting beam, made from longitudinal fibers

© 2021 Wiley-VCH GmbH

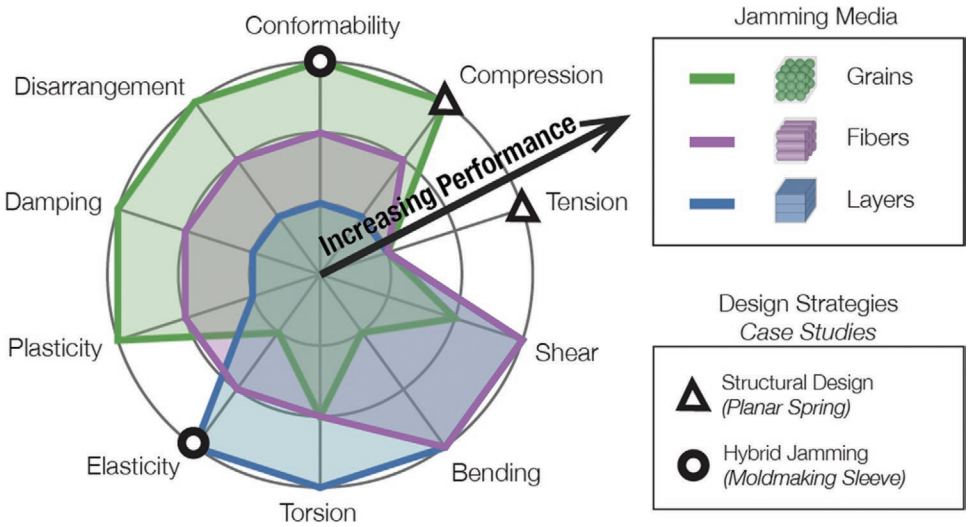

Figure 7. Design space of jamming structures based on performance metrics. The spider plot shows how the design space is spanned by the three different jamming media, giving designers and engineers the opportunity to choose the right jamming media for a particular application. The case studies presented in the previous section are presented as data points to show how the proposed design strategies expand the design space: combining grains and layers to achieve both conformability and elasticity, and designing a planar spring to achieve variable stiffness under tension and compression.

surrounded by grains, would have continuously-variable bending stiffness, structural integrity in bending due to fibers, and immediate energy dissipation due to grains.

These generalizable design strategies, along with the comparative mechanical analysis of the different jamming structures, provide a forward modeling framework that enables engineers to qualitatively predict the performance of a particular jamming structure under a particular loading condition. Although this paper provides guidelines for the design and analysis of a large variety of jamming structures, we are still far from developing a definitive design tool.

The categorization of the kinematic and frictional deformation modes is instructive and allows for a qualitative assessment of the mechanical behavior. However, a detailed quantitative understanding has not been achieved yet for either deformation mode. For the frictional mode, even though the behavior (e.g., conditions of slip, the stiffness before slip) is clearly defined, a consistent match between theoretical models and empirical results has not yet been achieved across scales, materials, and geometries. Moreover, boundary conditions (i.e., how these structures are anchored and loaded) have a large influence on how slip occurs and propagates throughout a structure. This topic has been studied for layer jamming structures in bending,[10] but not yet for fiber jamming structures in bending or layer jamming structures in torsion. For the kinematic deformation mode, matching the empirical results to theoretical models has also been challenging, as many models rely on extensive idealizations such as frictionless contact and rigid constituents. In addition, experiments yield less repeatable behavior, as most structures have a random arrangement of grains or fibers. Researchers have included a cyclic "preloading" step during their mechanical characterization experiments for granular jamming in order to achieve more repeatable stiffness values.[66,67] Furthermore, the significant impact of the membrane, especially when it conforms to the internal fibers or grains, has been investigated by only a small number of studies.[40,63]

This paper attempts to provide a forward modeling framework that connects the diverse work on jamming phenomena in the literature. The framework can help to illuminate the gaps in theoretical understanding of jamming. In addition, by looking at constituent-level interactions, it connects design decisions to mechanical performance. The framework is then utilized in two design strategies, demonstrated through two case studies in which a desired performance is achieved. Altogether, this paper may establish a foundation for developing quantitative design methodologies for jamming structures.

4. Experimental Section

Jamming-Based Planar Springs: A new fabrication methodology was developed in order to create jamming-based planar springs with complex geometries. First, layers of ordinary printer paper were cut into patterns using a laser cutter. These layers were then stacked and encased in an airtight thermoplastic urethane film (Strechlon 200, Fibre Glast Developments Corp, OH, USA). Thermoelastic urethane tubing (TPU1-2N, Eldon James, CO, USA) was heat-welded to the envelope to ensure an airtight connection to a vacuum pump. After a fully airtight encasing was achieved using a tacking iron or an impulse sealer, the internal sections surrounding the flexible elements also need to be bonded. The laser cutter was used for the bonding as well. The structure was placed into the laser-cutter in its jammed state to ensure that the top and bottom TPU film layers were flushed with each other. The laser was defocused by 44.5 mm and a bonding pattern was used to laser-bond the two films throughout the internal sections. Then, the laser was refocused to cut out the leftover film. This new repeatable fabrication methodology introduced opportunities to create high-precision layer-jamming structures (See Video S2, Supporting Information).

The performance of the planar springs was tested using the experimental setup in Figure 5B. The spring was attached to a fixture using a circular clamp along its rim. This fixture was then attached to a six-axis force/torque (F/T) sensor (Mini 40, ATI Industrial Automation, NC, USA) which was clamped to a flat surface. The middle portion of the spring was attached to a small vertical structure which was used to both apply forces to the spring and to attach optical tracking fiducials. Data were collected for three separate loading conditions: tension and

© 2021 Wiley-VCH GmbH

compression, and positive and negative rotation in two orthogonal directions. Each condition had four separate trials. The load was applied manually as a point load either by pulling with a string or by pushing with a needle. Load and position data were recorded simultaneously using the F/T sensor and a visual tracking system (fusionTrack500, Atracsys LLC, Puidoux, Switzerland). The tracking system allowed the extraction of both the 3D position as well as the orientation. The recorded load and position data were aligned manually, and the trials were interpolated and averaged. The stiffnesses were extracted using a spline fit to the average curves.

Hybrid Jamming-Based Mold-Making Sleeve: Three mold-making sleeves of the same scale were fabricated using coffee grounds and printer paper in an airtight envelope: one with only coffee grounds, one with only paper, and one with both, but with the layers on the outer side of the sleeve (Figure 6). For the envelope, a thin thermoplastic urethane film (thickness of 0.025 mm) was used in order to minimize the effect of the envelope on surface definition.

The three sleeves were then used to create molds and casts using the same process, which is shown both in Figure 6 and Video S3, Supporting Information. The unjammed sleeve was wrapped around the object and secured with rubber bands. The sleeve was then jammed by applying a vacuum. Then, the rubber bands were removed and the sleeve was bent open to remove the object. Afterward, a casting material (in this case, plaster) was used to fill the internal surface of the mold. After the plaster sets, the sleeve was unjammed and peeled off to expose the cast of the original object.

The mold-making sleeves' performances were experimentally measured for quantitative comparison. First, a hand-held high-resolution 3D scanner (Artec Space Spider, Artec, Luxembourg) was used to scan the original object and resulting casts from all directions. The extracted STL files of the objects were then used to create point clouds. After an initial manual alignment of each cast with the original object and removal of extraneous points, an iterative closest point algorithm was used to refine the alignment and extract the root mean square error for the two point clouds. The error was also calculated per-point to visualize the localized accuracies of the resulting casts, as shown in Figure 6 in the rightmost column.

Supporting Information

Supporting Information is available from the Wiley Online Library or from the author.

Acknowledgements

Authors would like to thank John Hutchinson, James Weaver, Joost Vlassak, Jeremy Axel Guillette, Lara Tomholt, Christopher Payne, Fedor Sirota, and Oliver Dana Strand for their valuable suggestions and feedback, as well as assistance with data processing. Authors would also like to thank the reviewers for their thorough and insightful feedback. This study was funded by the U.S. National Science Foundation National Robotics Initiative Grant CMMI-1637838.

Conflict of Interest

The authors declare no conflict of interest.

Keywords

hybrid materials, jamming, metamaterials, structure–property relationships, variable stiffness

Received: September 3, 2020
Revised: December 21, 2020
Published online:

[1] B. Vanderborght, A. Albu-Schäffer, A. Bicchi, E. Burdet, D. G. Caldwell, R. Carloni, M. G. Catalano, O. Eiberger, W. Friedl, G. Ganesh, M. Garabini, *Robot. Auton. Syst.* **2013**, *61*, 1601.
[2] Y. Yang, Y. Li, Y. Chen, *Bio-Des. Manuf.* **2018**, *1*, 14.
[3] M. Manti, V. Cacucciolo, M. Cianchetti, *IEEE Robot. Autom. Mag.* **2016**, *23*, 93.
[4] L. Wang, Y. Yang, Y. Chen, C. Majidi, F. Iida, E. Askounis, Q. Pei, *Mater. Today* **2018**, *21*, 563.
[5] S. Wolf, G. Grioli, O. Eiberger, W. Friedl, M. Grebenstein, H. Höppner, E. Burdet, D. G. Caldwell, E. Carloni, M. G. Catalano, D. Lefeber, *IEEE/ASME Trans. Mechatronics* **2015**, *21*, 2418.
[6] S. G. Fitzgerald, G. W. Delaney, D. Howard, *Actuators* **2020**, *9*, 104.
[7] H. M. Jaeger, *Soft Matter* **2015**, *11*, 12.
[8] M. Cianchetti, T. Ranzani, G. Gerboni, T. Nanayakkara, K. Althoefer, P. Dasgupta, A. Menciassi, *Soft Robot.* **2014**, *1*, 122.
[9] M. Brancadoro, M. Manti, S. Tognarelli, M. Cianchetti, *Soft Robot.* **2020**, *7*, 663.
[10] Y. S. Narang, J. J. Vlassak, R. D. Howe, *Adv. Funct. Mater* **2018**, *28*, 1707136.
[11] E. Brown, N. Rodenberg, J. Amend, A. Mozeika, E. Steltz, M. R. Zakin, H. Lipson, H. M. Jaeger, *Proc. Natl. Acad. Sci. U. S. A.* **2010**, *107*, 18809.
[12] E. Steltz, A. Mozeika, N. Rodenberg, E. Brown, H. M. Jaeger, in *2009 IEEE/RSJ Int. Conf. on Intelligent Robots and Systems*, IEEE, Piscataway, NJ **2009**, 5672.
[13] A. A. Stanley, J. C. Gwilliam, A. M. Okamura, in *World Haptics Conf. (WHC)*, IEEE, Piscataway, NJ **2013**, 25.
[14] B. Aktaş, R. D. Howe, in *IEEE Int. Conf. on Soft Robotics (RoboSoft)*, IEEE, Piscataway, NJ **2020**, 879.
[15] M. Brancadoro, M. Manti, F. Grani, S. Tognarelli, A. Menciassi, M. Cianchetti, *Front. Robot. AI* **2019**, *6*, 12.
[16] Y. S. Narang, A. Degirmenci, J. J. Vlassak, R. D. Howe, *IEEE Robot. Autom. Lett.* **2017**, *3*, 688.
[17] Y. J. Kim, S. Cheng, S. Kim, K. Iagnemma, *IEEE Trans. Robot.* **2013**, *29*, 1031.
[18] J. Ou, L. Yao, D. Tauber, J. Steimle, R. Niiyama, H. Ishii, in *TEI '14: Proceedings of the 8th Int. Conf. on Tangible, Embedded and Embodied Interaction*, Association for Computing Machinery, New York **2014**, 65.
[19] Y. S. Narang, B. Aktaş, S. Ornellas, J. J. Vlassak, R. D. Howe, *Soft Robot.* **2020**, *7*, 724.
[20] N. Vasios, Y. S. Narang, B. Aktaş, R. D. Howe, K. Bertoldi, *Eur. J. Mech. A - Solids* **2019**, *75*, 322.
[21] D. Bi, J. Zhang, B. Chakraborty, R. P. Behringer, *Nature* **2011**, *480*, 355.
[22] E. J. Banigan, M. K. Illich, D. J. Stace-Naughton, D. A. Egolf, *Nat. Phys.* **2013**, *9*, 288.
[23] A. J. Liu, S. R. Nagel, *Nature* **1998**, *396*, 21.
[24] A. J. Liu, S. R. Nagel, *Annu. Rev. Condens. Matter Phys.* **2010**, *1*, 347.
[25] J. N. Roux, *Phys. Rev. E* **2000**, *61*, 6802.
[26] M. van Hecke, *J. Phys.: Condens. Matter* **2009**, *22*, 033101.
[27] T. Mitsuda, in *World Haptics Conf. (WHC)*, IEEE, Piscataway, NJ **2017**, 364.
[28] V. Wall, R. Deimel, O. Brock, in *IEEE Int. Conf. on Robotics and Automation*, IEEE, Piscataway, NJ **2015**, 252.
[29] M. Langer, E. Amanov, J. Burgner-Kahrs, *Soft Robot.* **2018**, *5*, 291.
[30] E. Lathrop, I. Adibnazari, N. Gravish, M. T. Tolley, in *IEEE Int. Conf. on Soft Robotics (RoboSoft)*, IEEE, Piscataway, NJ **2020**, 388.
[31] P. M. Loschak, S. F. Burke, E. Zumbro, A. R. Forelli, R. D. Howe, in *IEEE/RSJ Int. Conf. on Intelligent Robots and Systems*, IEEE, Piscataway, NJ **2015**, 216.
[32] M. S. Moses, M. D. Kutzer, H. Ma, M. A. Armand, in *IEEE Int. Conf. on Robotics and Automation*, IEEE, Piscataway, NJ **2013**, 4008.
[33] R. Mukaide, M. Watanabe, K. Tadakuma, Y. Ozawa, T. Takahashi, M. Konyo, S. Tadokoro, *IEEE Robot. Autom. Lett.* **2020**, *5*, 5221.
[34] I. Choi, N. Corson, L. Peiros, E. W. Hawkes, S. Keller, S. Follmer, *IEEE Robot. Autom. Lett.* **2017**, *3*, 450.

 © 2021 Wiley-VCH GmbH

[35] W. H. Choi, S. Kim, D. Lee, D. Shin, *IEEE Robot. Autom. Lett.* **2019**, *4*, 2539.
[36] I. Albert, J. G. Sample, A. J. Morss, S. Rajagopalan, A. L. Barabási, P. Schiffer, *Phys. Rev. E.* **2001**, *64*, 061303.
[37] S. Kawamura, T. Yamamoto, D. Ishida, T. Ogata, Y. Nakayama, O. Tabata, S. Sugiyama, in *IEEE Int. Conf. on Robotics and Automation*, IEEE, Piscataway, NJ **2002**, 248.
[38] N. G. Cheng, M. B. Lobovsky, S. J. Keating, A. M. Setapen, K. I. Gero, A. E. Hosoi, K. D. Iagnemma, in *IEEE Int. Conf. on Robotics and Automation*, IEEE, Piscataway, NJ **2012**, 4328.
[39] F. Huijben, F. Van Herwijnen, R. Nijsse, in *Structural Membranes* (Eds: E. Oñate, B. Kröplin), CIMNE, Stuttgart, Germany **2009**, p. 1.
[40] A. Jiang, G. Xynogalas, P. Dasgupta, K. Althoefer, T. Nanayakkara, in *IEEE/RSJ Int. Conf. on Intelligent Robots and Systems*, IEEE, Piscataway, NJ **2012**, 2922.
[41] M. Bureau, T. Keller, J. Perry, R. Velik, J. F. Veneman, in *IEEE Int. Conf. on Rehabilitation Robotics*, IEEE, Piscataway, NJ **2011**, 1.
[42] B. Aktaş, R. D. Howe, in *IEEE/RSJ Int. Conf. on Intelligent Robots and Systems*, IEEE, Piscataway, NJ **2019**, 7616.
[43] S. Hauser, M. Robertson, A. Ijspeert, J. Paik, *IEEE Robot. Autom. Lett.* **2017**, *2*, 849.
[44] A. R. Deshpande, Z. T. H. Tse, H. Ren, in *IEEE Int. Conf. on Robotics and Automation*, IEEE, Piscataway, NJ **2017**, 417.
[45] Y. Yang, Y. Zhang, Z. Kan, J. Zeng, M. Y. Wang, *Soft Robot.* **2019**, *7*, 292.
[46] J. L. C. Santiago, I. S. Godage, P. Gonthina, I. D. Walker, *Soft Robot.* **2016**, *3*, 54.
[47] Y. Jiang, D. Chen, C. Liu, J. Li, *Soft Robot.* **2019**, *6*, 118.
[48] Y. Zhou, L. M. Headings, M. J. Dapino, in *IEEE Int. Conf. on Robotics and Automation*, IEEE, Piscataway, NJ **2019**, 6124.
[49] S. B. Diller, S. H. Collins, C. Majidi, *J. Intell. Mater. Syst. Struct.* **2018**, *29*, 3804.
[50] Y. Okatani, T. Nishida, K. Tadakuma, in *Joint 7th Int. Conf. on Soft Computing and Intelligent Systems (SCIS) and 15th Int. Symp. on Advanced Intelligent Systems (ISIS)*, IEEE, Piscataway, NJ **2014**, 231.
[51] B. H. Do, V. Banashek, A. M. Okamura, *arXiv:2002.04728*, **2020**.
[52] F. P. Beer, E. R. Johnston, J. T. DeWolf, *Mechanics of Materials*, McGraw-Hill, New York, NY **2012**.
[53] Y. Zhao, J. Barés, H. Zheng, C. S. Bester, Y. Xu, J. E. Socolar, R. P. Behringer, *Granular Matter* **2019**, *21*, 90.
[54] T. Börzsönyi, R. Stannarius, *Soft Matter* **2013**, *9*, 7401.
[55] N. Weiner, Y. Bhosale, M. Gazzola, H. King, *J. Appl. Phys.* **2020**, *127*, 050902.
[56] T. A. Marschall, *Ph.D. The Role of Particle Shape in Granular Rheology and Jamming*, University of Rochester **2020**.
[57] K. A. Murphy, K. A. Dahmen, H. M. Jaeger, *Phys. Rev. X* **2019**, *9*, 011014.
[58] S. Pillitteri, G. Lumay, E. Opsomer, N. Vandewalle, *Sci. Rep.* **2019**, *9*, 7281.
[59] A. K. Matsushita, L. Garcia, Z. Liu, J. Doan, M. A. Meyers, J. McKittrick, *J. Mater. Res. Technol.* **2020**, *9*, 15555.
[60] D. S. Shah, E. J. Yang, M. C. Yuen, E. C. Huang, R. Kramer-Bottiglio, *Adv. Funct. Mater.* **2020**, *31*, 2006915.
[61] D. M. Aukes, B. Heyneman, J. Ulmen, H. Stuart, M. R. Cutkosky, S. Kim, P. Garcia, A. Edsinger, *Int. J. Robot. Res.* **2014**, *33*, 721.
[62] T. Wang, J. Zhang, Y. Li, J. Hong, M. Y. Wang, *IEEE/ASME Trans. Mechatronics* **2019**, *24*, 424.
[63] A. Jiang, T. Ranzani, G. Gerboni, L. Lekstutyte, K. Althoefer, P. Dasgupta, T. Nanayakkara, *Soft Robot.* **2014**, *1*, 192.
[64] K. Tanaka, M. A. Karimi, B. P. Busque, D. Mulroy, Q. Zhou, R. Batra, A. Srivastava, H. M. Jaeger, M. Spenko, in *IEEE Int. Conf. on Soft Robotics (RoboSoft)*, IEEE, Piscataway, NJ **2020**, 852.
[65] L. L. Howell, S. Thomson, J. A. Briscoe, J. J. Parise, S. Lorenc, J. B. Larsen, C. R. Huffmire, N. Burnside, T. A. Gomm (Birgham Young University), *U.S. Patent 6,983,924*, **2006**.
[66] L. Blanc, A. Pol, B. François, A. Delchambre, P. Lambert, F. Gabrieli, in *Micro to MACRO Mathematical Modelling in Soil Mechanics* (Eds: P. Giovine, P. M. Mariano, G. Mortara), Birkhäuser, Cham **2018**, p. 57.
[67] A. G. Athanassiadis, M. Z. Miskin, P. Kaplan, N. Rodenberg, S. H. Lee, J. Merritt, E. Brown, J. Amend, H. Lipson, H. M. Jaeger, *Soft Matter* **2014**, *10*, 48.

© 2021 Wiley-VCH GmbH